Finite element analysis of residual stress and warpage in a 3D printed semi-crystalline polymer: Effect of ambient temperature and nozzle speed

FINITE ELEMENT ANALYSIS OF RESIDUAL STRESS AND WARPAGE IN A 3D PRINTED SEMI-CRYSTALLINE POLYMER: EFFECT OF AMBIENT TEMPERATURE AND NOZZLE SPEED

Anto Antony Samy[a]*, Atefeh Golbang[a], Eileen Harkin-Jones[a], Edward Archer[a], David Tormey[b], Alistair McIlhagger[a]

a: Engineering Research Institute, Ulster University, Shore Road, Newtownabbey, Co. Antrim, BT37 0QB, United Kingdom

b: Centre for Precision Engineering, Materials and Manufacturing Research, Institute of Technology Sligo, Ash Lane, F91 YW50 Sligo, Ireland

Abstract

The printing conditions in Fused Deposition Modelling (FDM) affect the amount of induced residual stresses within the printed part and its dimensional accuracy. Among the thermoplastic feedstock for FDM, semi-crystalline polymers are more prone to part distortion due to crystallisation. Therefore, this study aims to numerically investigate the behaviour of semi-crystalline polymer under various FDM printing conditions (namely print speed and ambient temperature) and the resultant residual stress and warpage in the printed parts. For this, the coefficient of thermal expansion (CTE) and the thermo-mechanical properties of the polymer under study (polypropylene), and the crystallisation kinetics are coupled with the evolving temperature and time during printing. The values of residual stress and warpage are calculated and compared for the bottom and top layers of the samples. From the results, it was observed that increasing the nozzle speed from 30mm/s to 60mm/s resulted in the bottom and top layers exhibiting a 15% and 13% decrease in residual stress, respectively. Similarly, a drop in warpage (~30%) was observed for both layers. The reduction in residual stress and warpage with increased printing speed is attributed to the improved heat transfer between the deposited roads and the reduced cooling rate. Increasing the ambient temperature from 25°C to 75°C resulted in a 2% and 3% decrease in residual stress in the bottom and top layers, respectively. In terms of warpage, an insignificant increase (~1%) was observed in both top and bottom layers. This is explained by the counter effects of reduced thermal gradients (i.e., lower cooling rate) and increased crystallisation on the overall amount of residual stress and warpage. 3D scanning of experimentally printed samples was used for verification of the simulation results, and good agreement between these is reported.

Keywords

Fused Deposition Modelling (FDM), Finite Element Analysis (FEA), Semi-crystalline polymers, Warpage, Residual stress, Polymer Crystallisation Kinetics.

1. Introduction

Even though Additive Manufacturing (AM) is progressing rapidly, only a few AM processes demonstrate the potential to accommodate the flexible requirements of industrial needs [1,2], one of which is Fused Deposition Modelling (FDM). Fused Deposition Modelling is an extrusion-based AM method in which the filament feedstock is transported through a liquefier into the moving nozzle where the material is melted and deposited on the print bed; the deposition pattern being driven by a 3D CAD model [3,4]. The feedstocks for FDM include mainly metals, ceramics and thermoplastic polymers, among which semi-crystalline polymers are gaining more attention in industrial applications due to their good mechanical and thermal properties [1,5]. However, due to the dense alignment of polymer chains in the lamella, semi-crystalline polymers are highly prone to residual stresses and shrinkage during the cooling phase after deposition [6]. Furthermore, the non-uniformity in cooling induces differential shrinkage in part, which results in warpage [7]. As a result of these morphological changes, the quality and the mechanical properties of a 3D printed semi-crystalline polymer strongly depend on the cooling conditions and the degree of crystallisation, influenced by the printing conditions [1,8]. In addition, changes in the build orientation and printing conditions can result in significant anisotropy in the 3D printed part [9].

Optimisation of printing conditions during FDM, such as print bed temperature, printing speed, nozzle temperature and diameter, layer height, bonding between the deposited layers, and the print bed and raster pattern, can minimise warpage in 3D printed parts [4,6,10,11]. However, considering the large number of printing variables involved in FDM, optimisation of printing conditions for each material is complex and time-consuming using experimental methods. Hence, simulation and modelling can be applied to efficiently evaluate the effects of processing conditions on the printed part. Furthermore, numerical techniques provide the means to study the effects of these processing conditions with respect to crystallisation kinetics and thermo-mechanical behaviour of the printed polymer [10,12]. In recent years, several researchers have varied FDM parameters such as nozzle diameter, nozzle temperature, print speed, deposition of the first layer on the print bed, print bed temperature, ambient temperature, cooling rate and raster pattern to improve dimensional accuracy, print quality and material properties [3,5,13,14]. However, the effect of crystallisation on part distortion under various printing conditions has not been evaluated explicitly for semi-crystalline polymers in simulation studies.

In FDM, the thermal energy from the newly deposited road is transferred to the neighbouring roads and the substrate layers during the deposition process. Depending on the

printing conditions, the temperature distribution between the layers determine the degree of crystallisation and build-up of residual stresses in various parts of the print, resulting in differential warpage and anisotropic [15–17]. Zhang et al. investigated the thermal characteristics of parts printed in FDM and reported that, layer thickness and nozzle speed directly influence part distortion [14,18]. Their work laid the groundwork for future researchers and was considered pioneering in the FDM parameters' numerical investigation. Increasing nozzle speed resulted in high cooling rates as the deposited material was constantly reheated by a new deposit before it cooled down. Continuous reheating of the sample resembles annealing of the cooled layer where before the polymer is cooled to the bed temperature, it is reheated multiple times with the new road/layer deposition. Thus, releasing the built-in thermal stress and also restricting the polymer chains from achieving high molecular orientation. This was also seen in other experimental work [2,6,13,18–23]. Although, the final part quality and properties are affected by the temperature difference between the deposited polymer melt and the ambient temperature, this has only been studied by a few researchers. Reducing the gap between the ambient temperature and the melt temperature promotes a more homogenous heat transfer, which improves the bonding between the roads/layers. Based on experimental studies, parts printed with increased ambient temperature show improved mechanical properties [3,24–27].

In this work, the effect of printing conditions, namely, nozzle speed and ambient temperature, on the in-built residual stresses and warpage of a semi-crystalline polymer printed via FDM is simulated using COMSOL software and validated experimentally. To observe the effect of thermal gradients in the model along with the crystallisation phenomenon, the crystallisation kinetics of the semi-crystalline polymer and its thermo-mechanical properties are taken into account with respect to the temperature profile and printing time in FDM, depending on the printing conditions. This study is a continuation of our previous work, in which the effects of printing conditions such as bed temperature, raster pattern and layer thickness were investigated for an element selected from the bottom layer [28]. However, since the temperature distribution is non-uniform in the z-axis in FDM, in this work elements are selected from both bottom and top layers and analysed in terms of their relative crystallinity, warpage, and residual stresses.

2. Modelling

The model developed in this study includes solid mechanics, heat transfer and crystallisation physics, which are coupled with respect to the temperature evolving within the system as illustrated in Figure 1. This allows the model to simulate the transient nature of the temperature of a printed sample in the FDM process. Furthermore, the developed model considers several factors such as effect of gravity on the melt during its deposition, heat transfer between roads and the deposited layers [15], ambient temperature, and viscoelasticity of the polymer. To reduce the simulation time and simplify the process, sample dimensions of 50x50x2mm were considered in this study.

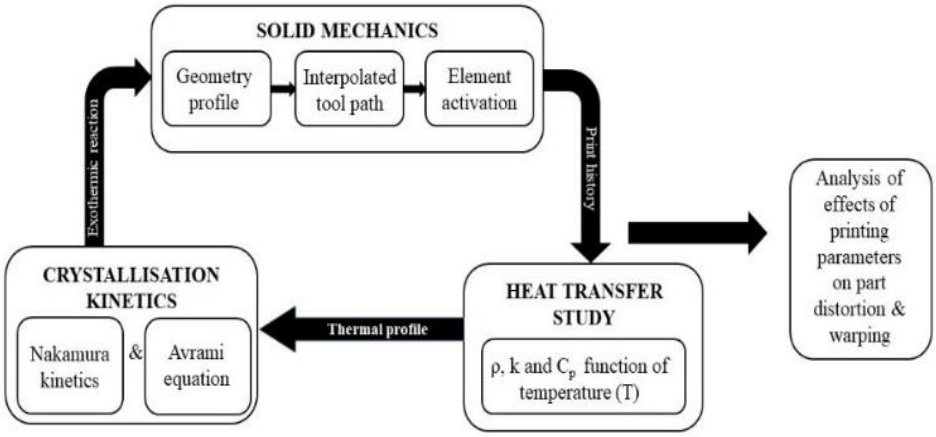

Figure 1. Process simulation plan

2.1. Solid mechanics

In this study, the elements in the simulated model are activated with respect to the material deposited during the printing process as shown in Figure 2. In this work, the raster pattern for the simulation study was developed in-house and integrated with the element activation technique. Initially, the model is meshed in correspondence with the road width extruded from the nozzle (0.5mm in this study), to activate the elements accordingly with the material deposition. During the initial period of the simulation, when the elements are activated, the activation proceeds in the x and y-axis, once the first layer is completed, the activation continues to the next layer in the z-axis.

In order to investigate the effects of processing conditions on part distortion, it is essential to consider the boundary condition between the model and the print bed. To address the print bed conditions, a fixed temperature and spring foundation boundary condition is applied beneath the bottom layer of the simulated model. This approach was followed and reported by Courter et al. in their study, where the model was allowed to warp freely when it is cooled down to the ambient temperature [29].

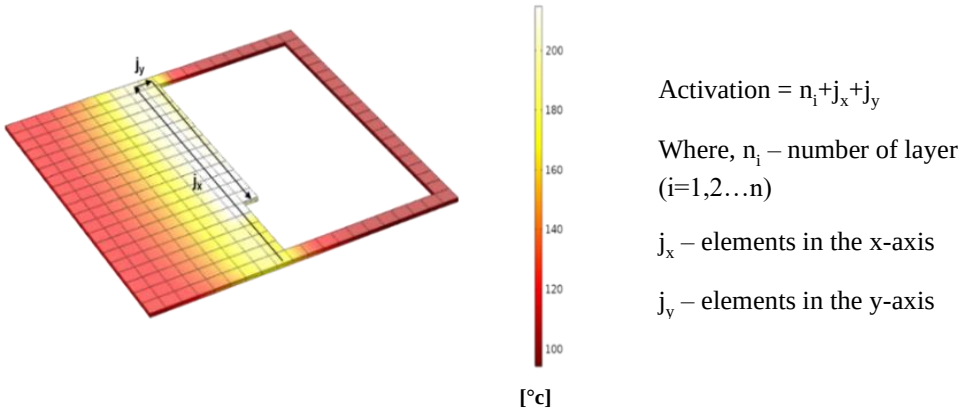

Figure 2. Element activation with respect to the material deposition process in FDM.

2.2. Heat transfer study

Researchers have emphasised the significance of the role of temperature in the FDM process [24]. Thermal conduction between the roads and layers plays a significant role in contributing to the bond strength of the printed sample [15,30]. Furthermore, the selection of processing parameters greatly influences the thermal profile of a printed sample and can have an adverse effect on part distortion [24,31,32]. Therefore in this study, the thermo-mechanical properties are expressed as a function of temperature (T) and also the physics incorporated in the model are coupled with respect to the evolving temperature of the system [33,34]. The following equation gives the general energy balance for heat transfer:

$$\rho C_p \frac{\partial T}{\partial t} - \nabla.(\lambda \nabla T) = Q \quad (1)$$

Where ρ is the density, $C_p$is the specific heat capacity and λ is the thermal conductivity of the polymer and Q is the heat source.

Additionally, in the developed model, pointwise constraint boundary condition was used, similar to the type of the constraint (spring foundation) boundary conditions used in the solid mechanics interface. Since the heat transfer study is coupled with the solid mechanics through temperature (T), the elements are activated at melt temperature with respect to the material deposition. During this activation, due to the coupling, the pointwise constraint acts on the nodes of the successfully activated elements of the model. Also, since crystallisation is an exothermic process, the heat dissipated during the crystallisation process was used as the heat source for the model. In terms of layer-to-layer interaction, since it is a continuum model, the heat dissipated from one layer transferred to the other layers. However, as aforementioned in section 2.1 (solid mechanics), spring foundation interface was used for the contact between the first layer and the print bed. The additional details of the model assumptions have been given in our previous work [28].

2.3. Crystallisation kinetics

Polymer crystallisation is a highly temperature dependent phenomenon that significantly affects a printed sample's part integrity [35,36]. Furthermore, the cooling rate applied to a semi-crystalline polymer can significantly affect the crystallisation process and subsequent mechanical properties of the polymer [37]. Therefore, physics developed by Levy [38], representing the crystalline nature of polymers, was modified and incorporated for semi-crystalline polymers.

Dressler et al. [39] and Wiria et al. [40] reported that the thermo-mechanical properties (C_p, ρ, λ) of a polymer are governed by heat transfer in the system. In addition, these thermo-mechanical properties also influence the crystallisation phenomenon of a polymer to a certain extent [38]. Therefore, in this study the thermo-mechanical properties, thermal conductivity (λ), specific heat capacity (C_p) and density (ρ), are expressed as a function of temperature (T) and assigned to the material property of the model [28,33,41].

Nakamura, taking into consideration non-isothermal crystallisation conditions, presented a theory derived from Avrami's equation [34]:

$$\alpha(t) = 1 - exp\left[-\int_0^t K(T)dt\right]^n \quad (2)$$

Where t is time, n is the Avrami index and *K*(T) is the Nakamura crystallisation kinetics function derived from Avrami's isothermal kinetics.

In an experimental study by Koscher et al. for both iso-thermal and non-isothermal conditions K(T) was modelled as [33,34,38]:

$$K(T) = \left(\frac{4}{3}\pi N_0(T)\right)^{\frac{1}{3}} G_0 * exp\left(-\frac{U^*}{R(T-T_\infty)}\right) exp\left(-\frac{K_g}{T(T_f-T)}\right) \quad (3)$$

The invoked equation in this model considers both time and temperature as driving factors, thus simulating the characteristics of the semi-crystalline polymer in the model. In this study, the employed Nakamura crystallisation kinetics model is widely recognised and used for simulating polymer crystallisation in modelling [42–46]. Detailed information on the equations assigned to calculate the crystallisation kinetics of the semi-crystalline polymer can be found in our previous paper [28].

3. Materials and methods

In this study, polypropylene (PP) was selected as the material of choice for simulation and experimental validation due to its commercial importance. Also, since PP belongs to the polyolefins group, it tends to crystallise faster with a high shrinkage rate which is a focus of this study [47]. The samples were simulated and experimentally printed with the following

printing parameters: nozzle diameter 0.8mm, print bed temperature of 100°C, line (90,90) raster pattern and infill of 100%. The extrusion temperature and the layer thickness in all cases were 210°C and 0.5mm, respectively. The processing parameters for the samples are presented in Table 1. In this study, the term nozzle speed indicates the printing speed of the FDM process, and ambient temperature is the temperature of the FDM chamber that is being maintained through the print. Here, sample a-Rs represents the reference sample, sample b-At represents the ambient temperature condition, and sample c-Ns represents the nozzle speed parameter.

Table 1. Processing parameters for PP

Processing conditions	**Ambient temperature (A_t) (°C)**	**Nozzle speed (N_s) (mm/s)**
Sample a-R_s	25	30
Sample b-A_t	75	30
Sample c-N_s	25	60

4. Results and discussion

The effects of different printing conditions on crystallisation and part distortion have been considered for two elements from the bottom (layer 1) and top (layer 4) of each sample. These selected elements will be referred to element 'n' and 'm' throughout the study as represented in Figure 3 (a) and (b). Element n was selected from the co-ordinates 7.8, 2.1 and 0.5 mm (layer 1), while element m was selected from the co-ordinates 7.8, 2.1 and 1.5mm (layer 4).

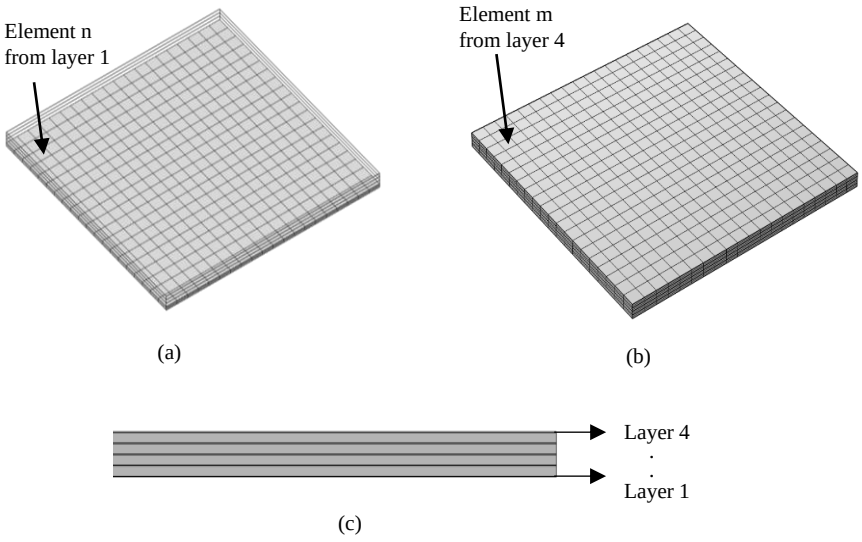

Figure 3. (a) Iso-metric view and location of element n in the printed part (b) Location of element m in the printed part (c) Side view of the printed part representing the layer sequence

4.1. Temperature evolution during printing

In the simulation, the material of study (polypropylene) was deposited on the print bed, allowing it to cool down to the bed temperature (100°C). Figure 4 (a) and (b) represent the changes in the temperature profile of elements n and m for the various printing conditions considered in this study. In Figure 4 (a), the prominent peaks represent the increase in temperature of element n due to the deposition of the subsequent layers (i.e., layers 2, 3 and 4). As the distance between layer 1 and the subsequent layers increases, the temperature rise in element n is reduced due to lower heat transfer.

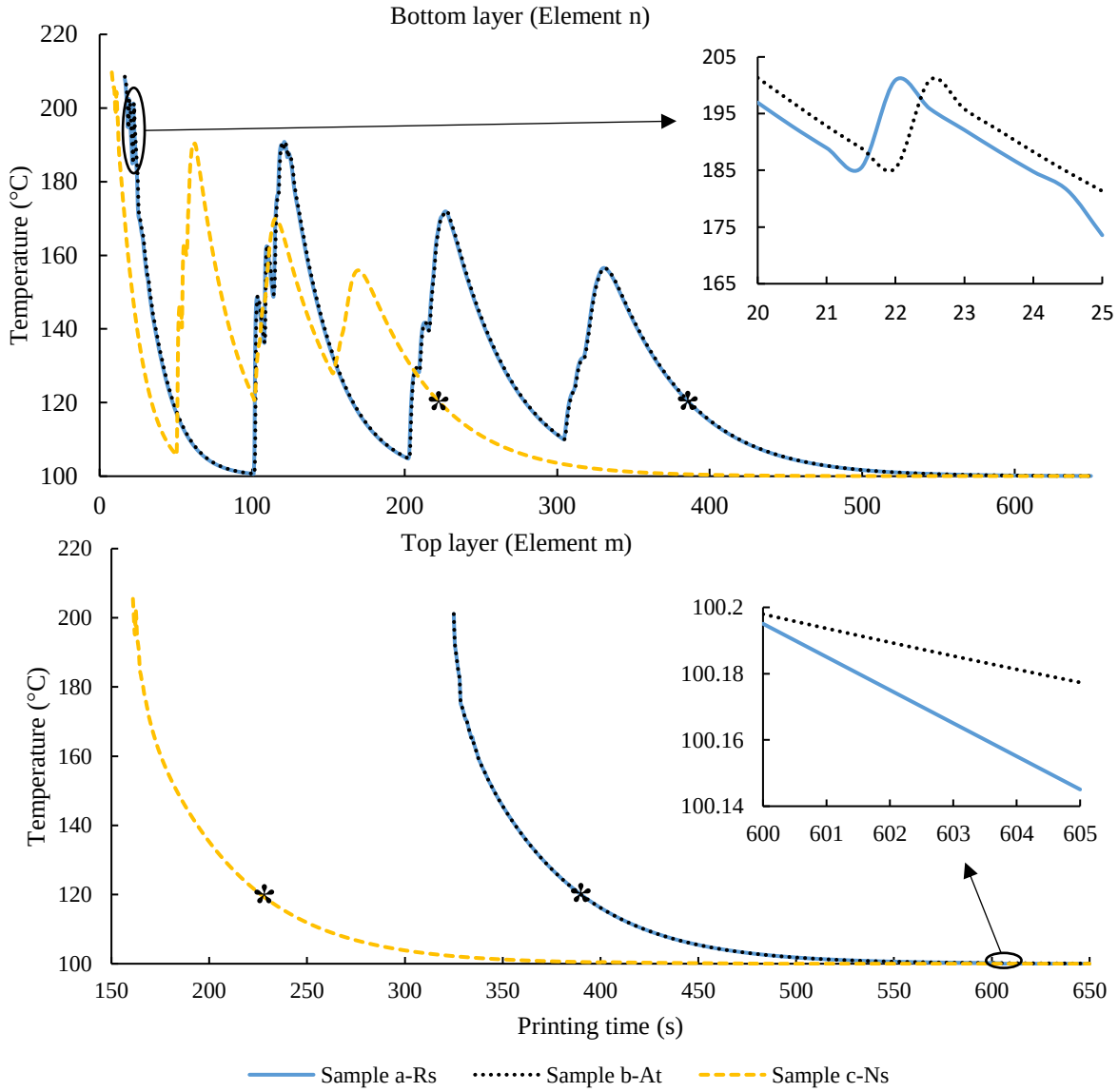

(b)

Figure 4. Comparison of the effects of thermal history from (a) the bottom layer (element n) and (b) top layer (element m) with respect to printing time of each layer at various printing conditions. The temperature distribution during the deposition of the bottom layer (element n) and the top layer (element m) of samples a-R_s, b-A_t and c-N_s are plotted against printing

time. An inset plot of sample a-Rs and b-At is magnified in (a) and (b) to show the temperature profile difference between the two samples.

Following melt deposition, minor peaks appear in the thermal profile of element n particularly in samples a-R_s and b-A_t which reflect the heat transfer from the adjacent neighbouring roads to element n [15,30,48]. This effect is continued to a certain extent as the subsequent layers are deposited. These minor peaks are not clearly visible in sample c-N_s due to the relatively shorter printing time in comparison to the other samples. Because of the increased nozzle speed, the newly deposited adjacent and neighbouring roads reheat element n more rapidly and prevent it from cooling down significantly (to low temperatures) in relation to the other two samples.

From the inset plot in Figure 4 (a) and (b), it can be seen that the cooling rate of elements n and m in sample b-A_t are slightly lower than that of the reference sample (a-R_s) as a result of increased ambient temperature [24,49]. It is also noticed that due to the increased printing speed in sample c-N_s, unlike element n (Figure 4 (a)), the cooling rate of element m is only slightly affected by the print speed (Figure 4 (b)). This is mainly because the rapid deposition at high print speeds of subsequent layers on top of the first layer decreases the overall cooling rate and temperature drop (i.e., loss of heat) in element n. However, when element m is deposited, the cooling rate of the sample is mainly controlled by its respective ambient temperature and the temperature of the third layer. The asterisks placed in Figure 4 (a) and (b) are discussed in the next section.

4.2. Effect of crystallisation

Generally, the crystallinity of the printed samples is hugely influenced by their cooling rate [47,50,51], which in turn depends on the printing conditions [13,23]. Therefore, to investigate the degree of crystallisation in relation to each printing condition, once the deposition process was completed, the relative crystallinity, built-in residual stress and warpage results of element n and m from all the samples were plotted at 120°C (Figure 5 (a) and (b)). The asterisks marked in Figure 4 (a) and (b) represent the points at which the simulation data for relative crystallinity, residual stress and warpage of the samples are taken.

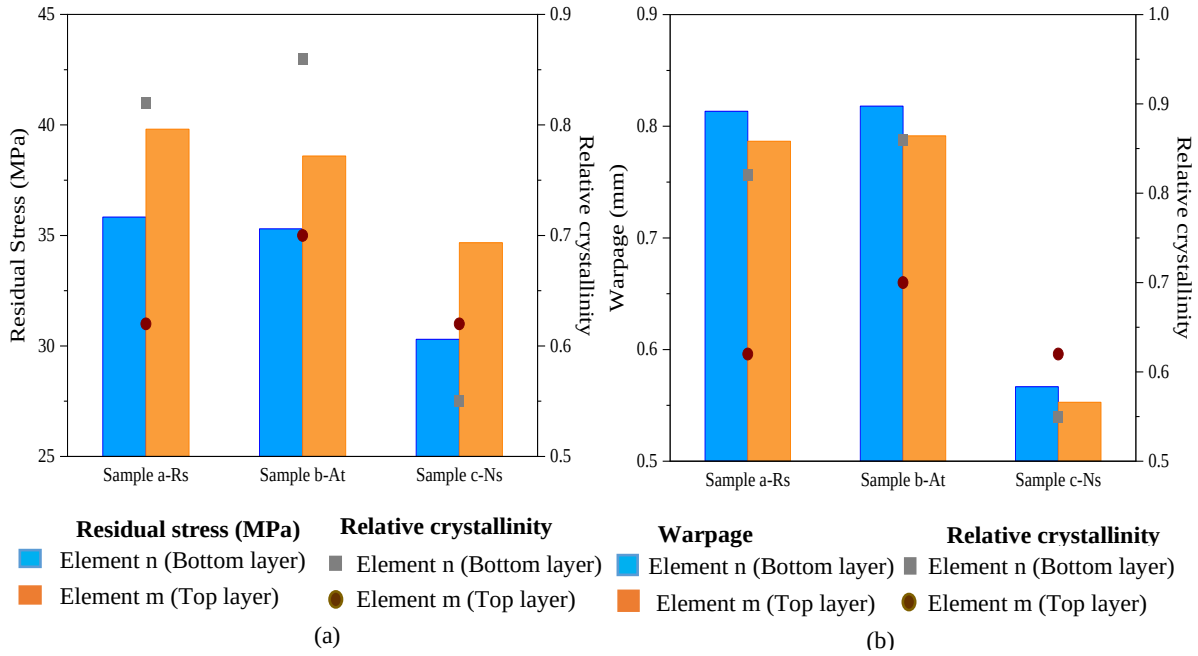

Figure 5. (a) Residual stress and relative crystallinity of element n and element m (b) Warpage and relative crystallinity of element n and element m at 120 ℃ plotted for samples a-R_s, b-A_t, and c-N_s with respect to different printing conditions.

As depicted in Figure 5 (a) and (b), among all the samples, the highest degree of crystallisation for elements n and m is achieved in sample b-A_t with the highest ambient temperature due to the lower cooling rate of the sample [17]. The higher crystallisation degree of element n compared with element m in samples a-R_s and b-A_t can be related to the multiple reheating of the bottom layer with further deposition of the subsequent layers, which can initiate re-crystallisation and cold crystallisation in this layer, while the top layer is merely exposed to the environment of the printing chamber and the previously deposited layer. [31,52]. Element n in sample c-N_s appears to exhibit the lowest degree of crystallinity among all, while element m in this sample has a similar crystallisation level as in element m in the reference sample. It can be proposed that, the decreased time of cooling (and reheating) and smaller temperature drop in the bottom layer of sample c-N_s hinders crystal formation and growth, resulting in a lower degree of crystallisation in element n. As this effect is more prominent in the bottom layer compared with the top layer, the level of crystallisation in element n is lower than that of element m for sample c-N_s. In fact, the cooling rate of element m in sample c-N_s is similar to that of the reference sample (with the same ambient temperature), which is why they both have similar levels of crystallisation (Figure 4 (b)) [13,25].

Interestingly, element n exhibits lower residual stress in all samples (Figure 5 (a)). This can be explained by the multiple reheating of the bottom layer during printing which releases

some residual stress. With an increase in ambient temperature from 25°C to 75°C, the bottom and top layers exhibit only a 2% and 3% decrease in residual stress, respectively. In terms of warpage, an insignificant increase (~1%) is observed in both the bottom and top layers. Commonly, residual stress occurs due to the variation in the temperature gradients during cooling [10]. This has previously been reported in an experimental study by Ferreira et al., where it was concluded that increased ambient temperature reduces residual stresses in the printed part due to the elimination of large thermal gradients [53]. This is also corroborated by the conclusions drawn by Zhang et al. from their experiments. Their study reported that increasing the ambient temperature resulted in the printed part achieving better inter-layer bonding with reduced internal stresses [54]. However, crystallisation kinetics in semi-crystalline polymers can also lead to residual stress accumulation, thereby resulting in warping [55,56]. Although increased ambient temperature reduces the build-up of thermal residual stress due to reduced thermal gradients, it simultaneously increases the crystallisation due to lower cooling, which on the contrary increases the amount of residual stress and warpage (because of the volumetric change governed by crystallisation). Hence, the two factors play a counterproductive role in the overall amounts of residual stress and warpage. In order to gain further insight into this phenomenon, the ambient temperature was further enhanced to 120°C under the same printing conditions in the simulation (data not reported here). For element n, the simulated model showed a decrease of 4.89% in residual stress and a 5.74% increase in warpage. For element m, the model depicted a significant drop of 14.76% in residual stress and a 6.21% rise in warpage. Hence, it is shown that by further increasing the ambient temperature to 120°C, there is an overall reduction in residual stress; however, it also leads to an increase in warpage due to an increase in crystallisation of the semi-crystalline polymer. In Figure 5 (a) and (b), although the built-in residual stress in element n among all the samples is higher than the stress found in element m, the relative crystallinity of element n is higher than m, which dictates the warpage. However, the elements from the bottom and top layer of sample c-N_s behave conversely to this explanation. This is because at 120°C, due to the increased nozzle speed, the values of the elements from sample c-N_s lie much ahead in printing time (x-axis) compared to the other samples. Additionally in sample c-N_s, the lower heat loss and lower crystallisation result in much lower values of residual stress and warpage compared with the other two samples [13,57]. Diederichs et al., Hallman et al. and Wang et al. have also reported that increasing the nozzle speed leads to reduced overall part cooling rate with multiple reheating's due to continuous layer deposition, which ultimately results in reduced part warpage [6,21,54].

4.3. Residual stress vs printing time

In Figure 6 (a) and (b), the residual stress profiles of element n and element m from all the samples were plotted against their overall printing time to study the evolution of stresses in the bottom and top layers under various printing conditions. The prominent peaks in the graphs in Figure 6 represents the deposition of each layer.

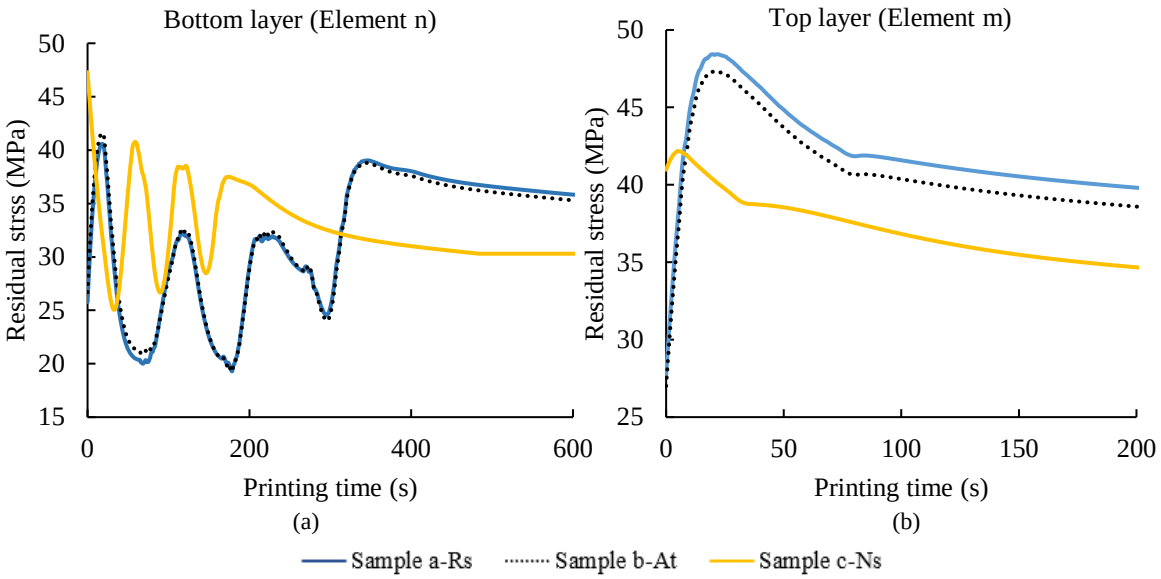

Figure 6. Comparison of residual stress distribution from (a) element n and (b) element m from sample a-R_s b-At, and c-Ns with each individual sample plotted against overall printing time. Every single peak represents each respective deposited layer in the printed sample.

Residual stress occurs during the printing process due to the continuous accumulation of trapped thermal stresses and volume changes (related to crystallisation in semi-crystalline polymers). As the deposited layer cools down and crystallisation takes place, the residual stresses develop and equilibrate. These built-in stresses are released due to the reheating generated by subsequent layer deposition. The prominent peaks observed in Figure 6 (a) represent the rise and fall of residual stress in element n due to its multiple reheating and cooling. For element m, the residual stress increases upon cooling and reaches an equilibrium state with time [30,48,58,59].

In Figure 6 (a), among the peaks observed in the samples, the first peak appears to be predominantly larger than the second and the third. This is because when the polymer melt is extruded onto the print bed, due to the large temperature difference between the first layer and the print bed, a steep increase in the residual stress is observed. Later, when this deposited melt is allowed to cool down, the deposited polymer starts relaxing and the residual stress built inside begins to gradually decrease [10]. The temperature difference between the next set of

deposited layers and the print bed is significantly lower; therefore, smaller changes (illustrated by peaks) are observed in the residual stress. Moreover, these newly deposited layers reheat the preceding layers resulting in the release of residual stress. It should be noted that reheating polymer layers could also result in re-crystallisation and cold crystallisation (depending on the temperature and polymer thermal properties), affecting the residual stresses inside the sample [31,52]. For example, element n in sample a-R_s undergoes re-crystallisation due to the reheating effect (as the reheating temperature from layer 2 reaches the crystallisation temperature of polypropylene). However, as the deposition progresses, the reheating effect from the higher layers causes cold crystallisation due to the smaller amount of heat transfer. Therefore, the cause of the final residual stress peak in the graphs (Figure 6 (a)) being greater in magnitude compared to the second and the third peaks is the higher amount of crystallisation achieved over time.

From Figure 6 (a) and (b), it is demonstrated that increasing the ambient temperature from 25°C to 75°C in sample b-A_t has slightly decreased the residual stresses when compared with the reference sample. The reason for such behaviour has been explained in detail in the previous section. The residual stress trend of both sample a-R_s and b-A_t appears to follow the same pattern but after the samples are allowed to cool to room temperature, the residual stresses in element n from sample b-A_t are reduced by 2%, and element m decreased by 3%. Here compared to element n, element m shows an additional 1% decrease in the predicted in-built residual in sample b-A_t. This is because, unlike element n, the cooling cycle of element m is not interrupted by layer depositions which allow the element to cool in relation to the ambient temperature.

As observed in Figure 6 (a) and (b), the development of residual stress is hindered in sample c-N_s due to the higher printing speed (60mm/s) and lower heat dissipation. In other words, sufficient time is not given for the temperature to drop and the residual stress to build up (as discussed explicitly in the previous section) [7,13,19]. Furthermore, the subsequent layers are deposited before the previous layer is cooled due to the increased deposition rate. Therefore, in sample c-N_s, even layer 4 seems to significantly affect the reheating of element n. Thus, increasing the nozzle speed in sample c-N_s, from 30 to 60mm/s, has demonstrated a 15% residual stress decrease from sample a-R_s. Whereas from Figure 6 (b), considering that element m is located on the top layer of the sample c-N_s, there is no reheating phenomenon, and also the sample cools down with respect to the ambient temperature processing condition, thus showing a 13% drop in residual stress compared to sample a-R_s. Watanabe et al. in their investigation on processing parameters on FDM, also reported that increasing the nozzle speed

has proved efficient in minimising warpage in their printed sample [23]. However, increasing the nozzle speed in simulation showed a considerable difference in the part distortion; a 60mm/s nozzle speed for PP in 3D printing was quite challenging to achieve as the deposited roads often broke due to the viscoelasticity of PP [60].

4.4. Warpage vs printing time

Warpage occurs due to the thermal contraction occurring in the printed samples due to accumulated residual stress in the printed sample [61]. The warpage results of elements n and m are plotted against their overall printing time (Figure 7) to examine the effects of printing conditions on the warpage.

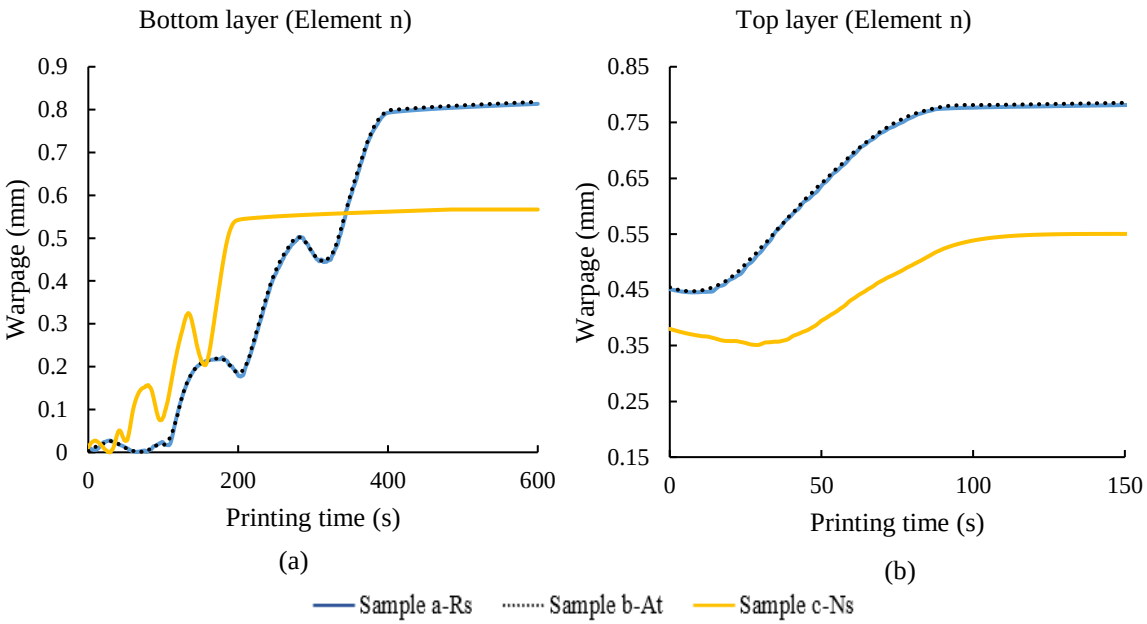

Figure 7. Warpage from (a) element n and (b) element m with respect to consequent layer deposition plotted against over all printing time. Every single peak representing each respective deposited layer in the printed sample.

From Figure 7 (a) and (b), it can be noted that warpage in all the samples appears to increase in a stepwise pattern along with their respective printing time. Following deposition, the printed layers start to cool down, but as mentioned in section 4.3, the warpage drops slightly due to the reheating effect from the newly deposited layers. In Figure 7 (b), it can be seen that initially the warpage of element m appears to originate as an almost flat line followed by a gradual increase and becomes stable again. The initial flat line in the graph indicates that the melt settles down when the layer is deposited. During the cooling process, once the melted polymer reaches the crystallisation temperature and the polymer chains start to crystallise, the sample begins to warp as it further cools [13,47,62]. As the samples cool down to

environmental (ambient) temperature, the overall warpage gradually stabilises in all the samples.

From Figure 7 (a) and (b), it is evident that samples a-R_s and b-A_t have the highest warpage among all the printed samples. It can be noted that even though increasing the ambient temperature from 25°C to 75°C appeared to be effective and slightly decreased the residual stresses, no significant difference is seen in the amounts of warpage between sample b-A_t and a-R_s. The reason for this has been explained in section 4.2. Sample c-N_s exhibits a faster rise and drop in the warpage value due to the increased nozzle speed. Increasing nozzle speed from 30 to 60mm/s allows the polymer to cool in a limited time period where the deposited polymer is reheated multiple times when the polymer chains are undergoing molecular orientation [7,13,23]. Continuous reheating of the adjacent deposited layers and decreased cooling time between the individual deposited layers results in minimum warpage in this sample [13,19].

4.5. Relationship between residual stresses and warpage

To understand and derive a relationship between the residual stress and warpage after completion of printing and cooling down of samples to ambient temperature, the final residual stress and overall warpage values of the samples printed under various printing conditions [32,61,63] were evaluated. The data is plotted in Figure 8.

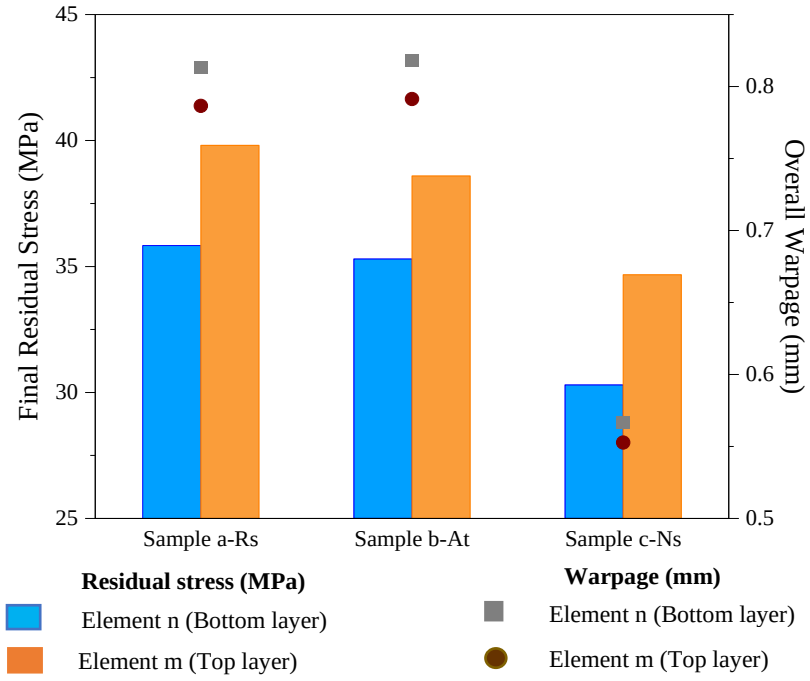

Figure 8. Ultimate residual stress from elements n and m in samples printed under various printed conditions are plotted against the final warpage to illustrate the effect of residual stress on part warpage.

According to Figure 8, element n in all samples shows higher warpage compared with element m. This difference becomes less evident with increased printing speed (30mm/s to 60mm/s). Interestingly, the amount of residual stress is in fact higher in element m (top layer) than in element n (bottom layer). It seems that crystallisation has a higher impact on warpage in this case. According to Chapman et al., residual stress is a product of the difference in the temperature gradients and does not depend entirely on the crystallisation state achieved by the polymer molecules [56]. Here in sample b-A_t, the decrease in thermal stress due to the increase in ambient temperature is over-shadowed by the stress accumulated from the crystallisation process, resulting in a slight drop in residual stress. In terms of warpage, despite the decrease in residual stress, the volumetric change that occurs due to the high degree of molecular crystallisation results in high warpage.

In general, an increase in ambient temperature (from 25°C to 75°C) and nozzle speed (from 30mm/s to 60mm/s) results in lower residual stress in both bottom and top layers. The effect of increased nozzle speed is more noticeable in this case.

4.6. Experimental validation

The simulated samples were printed using modified Ultimaker 2 under the processing parameters mentioned in section 3, and 3D scanned to assess the simulation results' validity under various printing conditions. A cartesian co-ordinate was constructed from the 3D scanned CAD model data for every measured model at (0,0,0) while two separate axes were created at the location elements n and m. The deviation values for element n were measured between the nominal axis (0,0,0) and the axis created at element n. For element m, a similar procedure was repeated to measure their respective warpage values.

The simulation results showed that increasing the ambient temperature from 25°C to 75°C leads to smaller amounts of increase in warpage due to the increased crystallisation of the polymer molecules. Adhesives such as adhesion-promoting sprays, glue, etc., are commonly employed during 3D printing to provide sufficient adhesion between the first layer and the print bed, and this can restrict the warpage in the first layer [11,64]. In the simulation, a spring foundation was used as the boundary condition between the first layer and the print bed to allow the model to warp. So, even though the developed simulation predicted warpage in the bottom layer of the simulated models, the printed samples showed very little warpage due to the usage of adhesive spray. Adhesion between the first few layers and the print bed influences the warpage rate in an FDM fabricated part. Hence, only the data for the top layer (element m) sample a-R_s and c-N_s are represented in Table 2. Since the material properties of

these adhesives were not considered in the current simulation, the predicted warpage of the bottom layer was inaccurate.

Table 2. Experimental validation of the simulated sample warpage of element m

Samples	Predicted warpage (FEA) (mm)	Measured warpage (Experimental) (mm)
Sample a-R_s	0.78	0.80
Sample c-N_s	0.55	0.52

From Table 2, it can be concluded that the 3D scanned warpage measurement data of the top layer appears to be in excellent agreement with the simulation results. This can be explained by considering the bonding between the sample and the print bed.

Furthermore, the temperature gradients of sample a-R_s and c-N_s were validated using the thermal camera, Bosch GTC 400C professional. From Figure 9, it can be seen that the FEA predictions and the reading from the IR camera show very similar trends for the thermal history of these two samples.

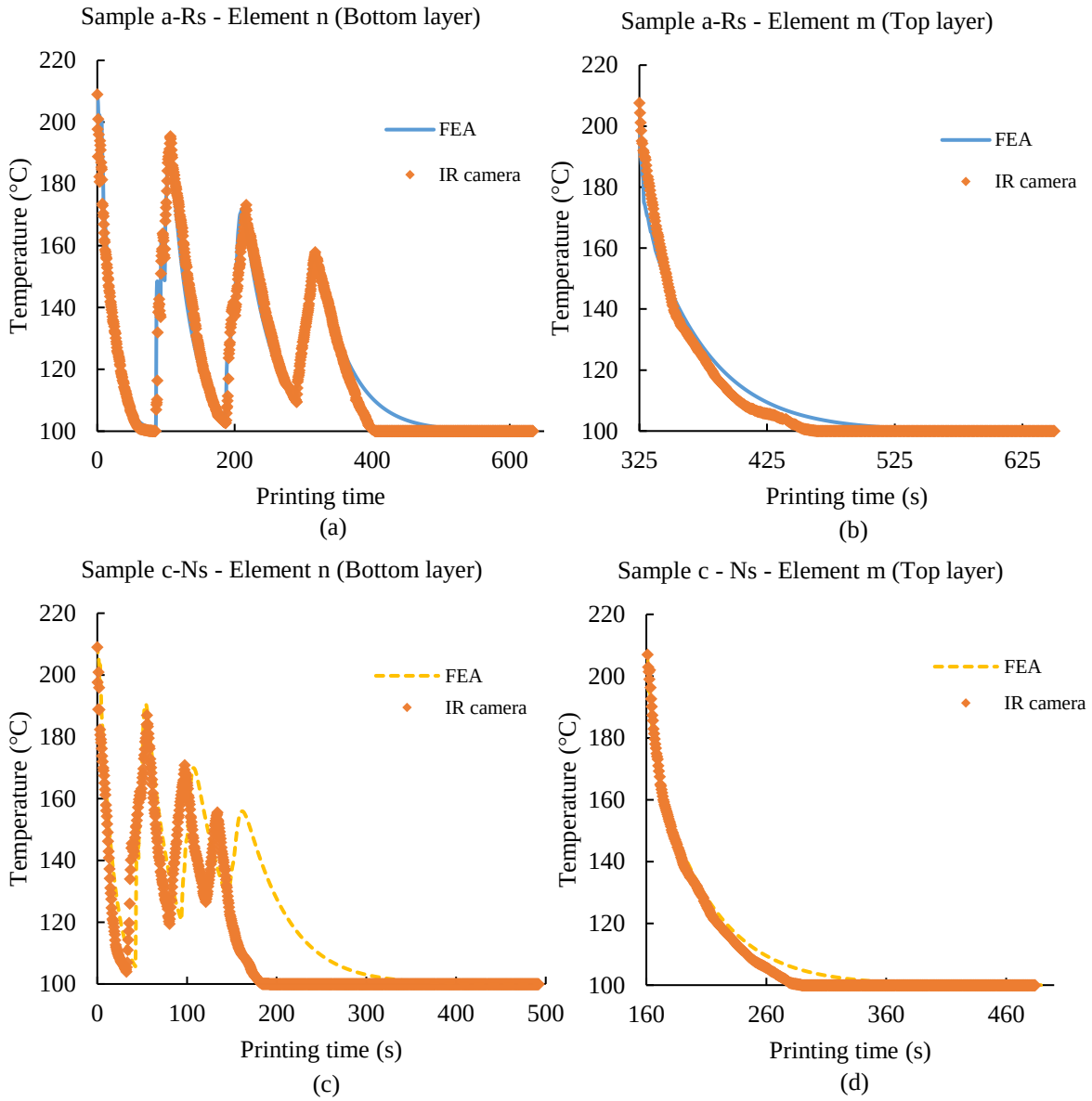

Figure 9. Comparison of FEA predicted thermal history of the samples against experimentally measured temperature gradients.

Figure 10 represents thermal images of temperature distribution of sample a-R_s (reference sample) at different time scales. Post completion of the printing process, it is evident (Figure 10) that the sample a-R_s (reference sample) starts to cool from outside while still retaining the thermal pool in the centre region. Due to this, the corners of the FDM printed samples are more prone to warpage.

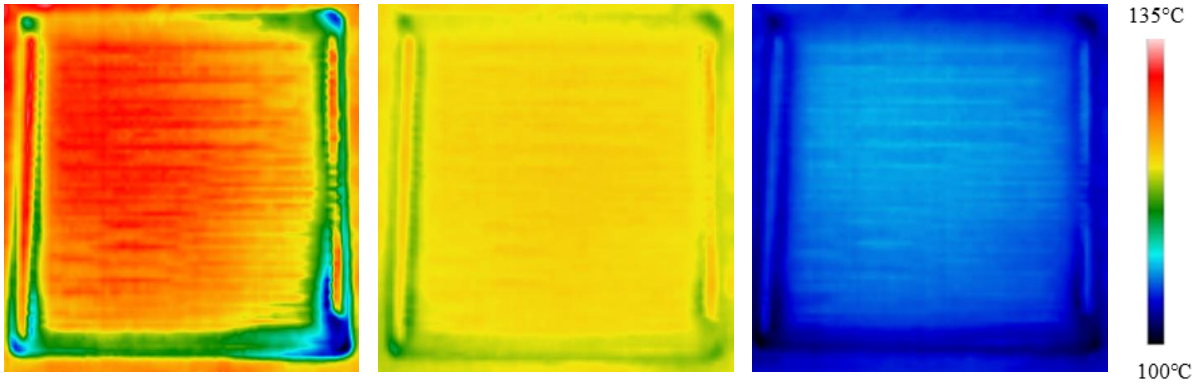

Figure 10. Thermal image showing temperature distribution in sample a-Rs (reference sample) after the completion of the printing process.

5. Conclusion

In this study, a transient 3D thermal model was developed to analyse the effect of different printing parameters (ambient temperature, number of layers and nozzle speed) on part distortion. The developed simulation can predict the residual stresses and warpage for any point in the printed model under various printing conditions (e.g., changes in ambient temperature, nozzle speed, layer thickness, bed temperature and raster patterns). In addition, the model accounts for factors such as temperature driven material properties, viscoelasticity, gravity, and the crystallinity of the polymer.

A detailed and in-depth study was performed on the effect of printing conditions on crystallisation and thermal history of the models and their impact on part distortion. The simulated models were experimentally printed and scanned to validate the simulation results. From the study, the following conclusions were drawn:

1. Increasing ambient temperature from 25°C to 75°C promotes bonding between the adjacent filaments and maintains a homogenous cooling condition thus reducing the induced thermal residual stresses. However, this can lead to an increase in the warpage of the printed samples due to the enhanced crystallisation of the polymer molecules.
2. Increasing nozzle speed from 30mm/s to 60mm/s can decrease the cooling time between the deposited filaments/layers, adversely affecting the crystallinity of the polymer and leading to low crystallisation. Additionally, the induced thermal stresses can be minimised due to the annealing effect from the newly deposited roads at a high printing rate. Therefore, optimised nozzle speed can be used to minimise the part distortion in the printed part.

6. Future work

In the next step of this study, the impact of filler particles and various raster patterns on warpage and residual stresses will be investigated.

7. Acknowledgements

The North West Centre for Advanced Manufacturing (NW CAM) project is supported by the European Union's INTERREG VA Programme, managed by the Special EU Programmes Body (SEUPB). The views and opinions in this document do not necessarily reflect those of the European Commission or the Special EU Programmes Body (SEUPB). If you would like further information about NW CAM please contact the lead partner, Catalyst, for details. I would also like to extend my thanks to Monali Dahale, Sean Duffy, William Moses and COMSOL for their support.

References

[1] Hertle S, Drexler M, Drummer D. Additive Manufacturing of Poly(propylene) by Means of Melt Extrusion. Macromol Mater Eng 2016;301:1482–93. https://doi.org/10.1002/mame.201600259.

[2] Wang TM, Xi JT, Jin Y. A model research for prototype warp deformation in the FDM process. Int J Adv Manuf Technol 2006;33:1087–96. https://doi.org/10.1007/s00170-006-0556-9.

[3] Spoerk M, Arbeiter F, Raguž I, Weingrill G, Fischinger T, Traxler G, et al. Polypropylene Filled With Glass Spheres in Extrusion-Based Additive Manufacturing: Effect of Filler Size and Printing Chamber Temperature. Macromol Mater Eng 2018;303. https://doi.org/10.1002/mame.201800179.

[4] Brenken B, Barocio E, Favaloro A, Kunc V, Pipes RB. Development and validation of extrusion deposition additive manufacturing process simulations. Addit Manuf 2019;25:218–26. https://doi.org/10.1016/j.addma.2018.10.041.

[5] Bakrani Balani S. Additive manufacturing of the high-performance thermoplastics: Experimental study and numerical simulation of the Fused Filament Fabrication. 2019.

[6] Diederichs E V., Picard MC, Chang BP, Misra M, Mielewski DF, Mohanty AK. Strategy to improve printability of renewable resource-based engineering plastic tailored for fdm applications. ACS Omega 2019;4:20297–307. https://doi.org/10.1021/acsomega.9b02795.

[7] Fischer JM. Handbook of Molded Part Shrinkage and Warpage: Second Edition. 2012. https://doi.org/10.1016/C2011-0-06800-X.

[8] Ruan C, Guo L, Liang K, Li W. Computer Modeling and Simulation for 3D

Crystallization of Polymers. II. Non-Isothermal Case. Polym - Plast Technol Eng 2012;51:816–22. https://doi.org/10.1080/03602559.2012.671413.

[9] Ahn SH, Montero M, Odell D, Roundy S, Wright PK. Anisotropic material properties of fused deposition modeling ABS. vol. 8. 2002. https://doi.org/10.1108/13552540210441166.

[10] El Moumen A, Tarfaoui M, Lafdi K. Modelling of the temperature and residual stress fields during 3D printing of polymer composites. Int J Adv Manuf Technol 2019:1661–76. https://doi.org/10.1007/s00170-019-03965-y.

[11] Spoerk M, Gonzalez-Gutierrez J, Sapkota J, Schuschnigg S, Holzer C. Effect of the printing bed temperature on the adhesion of parts produced by fused filament fabrication. Plast Rubber Compos 2018;47:17–24. https://doi.org/10.1080/14658011.2017.1399531.

[12] Ruan C. Kinetics and morphology of flow induced polymer crystallization in 3D shear flow investigated by Monte Carlo simulation. Crystals 2017;7. https://doi.org/10.3390/cryst7020051.

[13] Spoerk M, Holzer C, Gonzalez-Gutierrez J. Material extrusion-based additive manufacturing of polypropylene: A review on how to improve dimensional inaccuracy and warpage. J Appl Polym Sci 2019.

[14] Zhang Y, Chou Y. Three-dimensional finite element analysis simulations of the fused deposition modelling process. Proc Inst Mech Eng Part B J Eng Manuf 2006;220:1663–71. https://doi.org/10.1243/09544054JEM572.

[15] Costa SF, Duarte FM, Covas JA. Towards modelling of Free Form Extrusion: analytical solution of transient heat transfer. Int J Mater Form 2008;1:703–6. https://doi.org/10.1007/s12289-008-0356-x.

[16] Wolszczak P, Lygas K, Paszko M, Wach RA. Heat distribution in material during fused deposition modelling. Rapid Prototyp J 2018;24:615–22. https://doi.org/10.1108/RPJ-04-2017-0062.

[17] Li H, Wang T, Sun J, Yu Z. The effect of process parameters in fused deposition modelling on bonding degree and mechanical properties. Rapid Prototyp J 2018;24:80–92. https://doi.org/10.1108/RPJ-06-2016-0090.

[18] Zhang Y, Chou K. A parametric study of part distortions in fused deposition modelling using three-dimensional finite element analysis. Proc Inst Mech Eng Part B J Eng Manuf 2008;222:959–67. https://doi.org/10.1243/09544054JEM990.

[19] Xinhua L, Shengpeng L, Zhou L, Xianhua Z, Xiaohu C, Zhongbin W. An investigation

on distortion of PLA thin-plate part in the FDM process. Int J Adv Manuf Technol 2015;79:1117–26. https://doi.org/10.1007/s00170-015-6893-9.

[20] Jin M, Giesa R, Neuber C, Schmidt H. Filament Materials Screening for FDM 3D Printing by Means of Injection-Molded Short Rods 2018;1800507:1–7. https://doi.org/10.1002/mame.201800507.

[21] Hallmann M, Schleich B, Wartzack S. A method for analyzing the influence of process and design parameters on the build time of additively manufactured components. Proc. Int. Conf. Eng. Des. ICED, vol. 2019- Augus, 2019, p. 649–58. https://doi.org/10.1017/dsi.2019.69.

[22] Deng X, Zeng Z, Peng B, Yan S, Ke W. Mechanical properties optimization of poly-ether-ether-ketone via fused deposition modeling. Materials (Basel) 2018;11. https://doi.org/10.3390/ma11020216.

[23] Watanabe N, Shofner ML, Treat N, Rosen DW. A Model for Residual Stress and Part Warpage Prediction in. Solid Free. Fabr., 2016, p. 2437–55.

[24] Popescu D, Zapciu A, Amza C, Baciu F, Marinescu R. FDM process parameters influence over the mechanical properties of polymer specimens: A review. Polym Test 2018;69:157–66. https://doi.org/10.1016/j.polymertesting.2018.05.020.

[25] Sun Q, Rizvi GM, Bellehumeur CT, Gu P. Effect of processing conditions on the bonding quality of FDM polymer filaments. Rapid Prototyp J 2008;14:72–80. https://doi.org/10.1108/13552540810862028.

[26] Kumar S, Bhushan P, Sinha N, Prakash O, Bhattacharya S. Investigation of structure–mechanical property relationship in fused filament fabrication of the polymer composites. J Micromanufacturing 2019;2:167–74. https://doi.org/10.1177/2516598419843687.

[27] Zhang W, Wu AS, Sun J, Quan Z, Gu B, Sun B, et al. Characterization of residual stress and deformation in additively manufactured ABS polymer and composite specimens. Compos Sci Technol 2017;150:102–10. https://doi.org/10.1016/j.compscitech.2017.07.017.

[28] Antony Samy A, Golbang A, Harkin-Jones E, Archer E, McIlhagger A. Prediction of part distortion in Fused Deposition Modelling (FDM) of semi-crystalline polymers via COMSOL: Effect of printing conditions. CIRP J Manuf Sci Technol 2021;33:443–53. https://doi.org/10.1016/j.cirpj.2021.04.012.

[29] Courter B, Savane V, Bi J, Dev S, Hansen CJ. Finite Element Simulation of the Fused Deposition Modelling Process Modelling Process 2017.

[30] Mostafa N, Syed HM, Igor S, Andrew G. A Study of Melt Flow Analysis of an ABS-Iron Composite in Fused Deposition Modelling Process. Tsinghua Sci Technol 2009;14:29–37. https://doi.org/10.1016/S1007-0214(09)70063-X.

[31] Fitzharris ER, Watanabe N, Rosen DW, Shofner ML. Effects of material properties on warpage in fused deposition modeling parts. Int J Adv Manuf Technol 2018;95:2059–70. https://doi.org/10.1007/s00170-017-1340-8.

[32] Barocio E, Brenken B, Favaloro A, Bogdanor M, Pipes RB. Extrusion deposition additive manufacturing with fiber-reinforced thermoplastic polymers. Elsevier Inc.; 2020. https://doi.org/10.1016/b978-0-12-819535-2.00007-7.

[33] Brahmia N, Bourgin P, Boutaous M, Garcia D. Numerical simulation with "Comsol Multiphysics" of crystallization kinetics of semi-crystalline polymer during cooling: Application to injection moulding. Comsol Users Conf 2006:1–7.

[34] Koscher E, Fulchiron R. Influence of shear on polypropylene crystallization: Morphology development and kinetics. Polymer (Guildf) 2002;43:6931–42. https://doi.org/10.1016/S0032-3861(02)00628-6.

[35] Hu W, Zha L. Thermodynamics and kinetics of polymer crystallization. Polym Morphol Princ Charact Process 2016:242–58. https://doi.org/10.1002/9781118892756.ch13.

[36] Gradys A, Sajkiewicz P, Minakov AA, Adamovsky S, Schick C, Hashimoto T, et al. Crystallization of polypropylene at various cooling rates. Mater Sci Eng A 2005;413–414:442–6. https://doi.org/10.1016/j.msea.2005.08.167.

[37] Clark EJ. Molecular and Microstructural Factors Affecting Mechanical Properties of Polymeric Cover Plate Materials. 1985.

[38] Levy A. A Novel Physics Node for Nakamura Crystallization Kinetics. Int J Numer Methods Eng 2016. https://doi.org/10.1002/nme.

[39] Dressler M, Röllig M, Schmidt M, Maturilli A, Helbert J. Temperature distribution in powder beds during 3D printing. Rapid Prototyp J 2010;16:328–36. https://doi.org/10.1108/13552541011065722.

[40] Edith Wiria F, Fai Leong K, Kai Chua C. Modeling of powder particle heat transfer process in selective laser sintering for fabricating tissue engineering scaffolds. Rapid Prototyp J 2010;16:400–10. https://doi.org/10.1108/13552541011083317.

[41] Dos Santos WN, De Sousa JA, Gregorio R. Thermal conductivity behaviour of polymers around glass transition and crystalline melting temperatures. Polym Test 2013;32:987–94. https://doi.org/10.1016/j.polymertesting.2013.05.007.

[42] Boyard N. Heat Transfer in Polymer Composite Materials: Forming Processes. Heat Transf Polym Compos Mater Form Process 2016:1–434. https://doi.org/10.1002/9781119116288.

[43] Levy A, Le Corre S, Sobotka V. Heat transfer and crystallization kinetics in thermoplastic composite processing. A coupled modelling framework. AIP Conf Proc 2016;1769. https://doi.org/10.1063/1.4963594.

[44] Pignon B, Tardif X, Lefèvre N, Sobotka V, Boyard N, Delaunay D. A new PvT device for high performance thermoplastics: Heat transfer analysis and crystallization kinetics identification. Polym Test 2015;45:152–60. https://doi.org/10.1016/j.polymertesting.2015.05.013.

[45] Amado F, Wegener K, Schmid M, Levy G. Characterization and modeling of non-isothermal crystallization of Polyamide 12 and co-Polypropylene during the SLS process. 5th Int Polym Mould Innov Conf 2012:207–16.

[46] Le Goff R, Poutot G, Delaunay D, Fulchiron R, Koscher E. Study and modeling of heat transfer during the solidification of semi-crystalline polymers. Int J Heat Mass Transf 2005;48:5417–30. https://doi.org/10.1016/j.ijheatmasstransfer.2005.06.015.

[47] Dong M, Zhang S, Gao D, Chou B. The study on polypropylene applied in fused deposition modeling. AIP Conf Proc 2019;2065. https://doi.org/10.1063/1.5088317.

[48] Grimm T. Fused Deposition Modeling: A Technology Evaluation n.d.:1–12.

[49] Yu N, Sun X, Wang Z, Zhang D, Li J. Effects of auxiliary heat on warpage and mechanical properties in carbon fiber/ABS composite manufactured by fused deposition modeling. Mater Des 2020;195:108978. https://doi.org/10.1016/j.matdes.2020.108978.

[50] Nakamura K, Watanabe T, Katayama K, Amano T. Some aspects of nonisothermal crystallization of polymers. I. Relationship between crystallization temperature, crystallinity, and cooling conditions. J Appl Polym Sci 1972;16:1077–91. https://doi.org/10.1002/app.1972.070160503.

[51] Yamamoto T. Computer modeling of polymer crystallization - Toward computer-assisted materials' design. Polymer (Guildf) 2009;50:1975–85. https://doi.org/10.1016/j.polymer.2009.02.038.

[52] Furushima Y, Schick C, Toda A. Crystallization, recrystallization, and melting of polymer crystals on heating and cooling examined with fast scanning calorimetry. Polym Cryst 2018;1:1–10. https://doi.org/10.1002/pcr2.10005.

[53] Ferreira RTL, Quelho de Macedo R. Residual thermal stress in fused deposition

modelling 2018. https://doi.org/10.26678/abcm.cobem2017.cob17-0124.

[54] Zhang J, Wang XZ, Yu WW, Deng YH. Numerical investigation of the influence of process conditions on the temperature variation in fused deposition modeling. Mater Des 2017;130:59–68. https://doi.org/10.1016/j.matdes.2017.05.040.

[55] Parlevliet PP, Bersee HEN, Beukers A. Residual stresses in thermoplastic composites-A study of the literature-Part I: Formation of residual stresses. Compos Part A Appl Sci Manuf 2006;37:1847–57. https://doi.org/10.1016/j.compositesa.2005.12.025.

[56] Chapman TJ, Gillespie JW, Pipes RB, Manson JAE, Seferis JC. Prediction of Process-Induced Residual Stresses in Thermoplastic Composites. J Compos Mater 1990;24:616–43. https://doi.org/10.1177/002199839002400603.

[57] Fischer C, Drummer D. Crystallization and Mechanical Properties of Polypropylene under Processing-Relevant Cooling Conditions with respect to Isothermal Holding Time. Int J Polym Sci 2016;2016. https://doi.org/10.1155/2016/5450708.

[58] Bellini A, Güçeri S BM, Bellini A, Güçeri S, Bertoldi M. Liquefier Dynamics in Fused Deposition. J Manuf Sci Eng 2004;126(2):237. https://doi.org/10.1115/1.1688377.

[59] Dey A, Yodo N. A systematic survey of FDM process parameter optimization and their influence on part characteristics. J Manuf Mater Process 2019;3. https://doi.org/10.3390/jmmp3030064.

[60] Liu J, Anderson KL, Sridhar N. Direct Simulation of Polymer Fused Deposition Modeling (FDM) — An Implementation of the Multi-Phase Viscoelastic Solver in OpenFOAM. Int J Comput Methods 2020;17:1844002. https://doi.org/10.1142/s0219876218440024.

[61] Ji LB, Zhou TR. Finite Element Simulation of Temperature Field in Fused Deposition Modeling. Adv Mater Res 2010;97–101:2585–8. https://doi.org/10.4028/www.scientific.net/AMR.97-101.2585.

[62] Kantaros A, Karalekas D. Fiber Bragg grating based investigation of residual strains in ABS parts fabricated by fused deposition modeling process. Mater Des 2013;50:44–50. https://doi.org/10.1016/j.matdes.2013.02.067.

[63] Brenken B, Barocio E, Favaloro A, Kunc V, Pipes RB. Fused filament fabrication of fiber-reinforced polymers: A review. Addit Manuf 2018;21:1–16. https://doi.org/10.1016/j.addma.2018.01.002.

[64] Hämäläinen JP. Semi-Crystalline Polyolefins in Fused Deposition Modeling. 2017.